

“ A MICROWAVE PERFORMANCE CALIBRATION SYSTEM FOR NASA’S DEEP SPACE NETWORK ANTENNAS, PART 1: ASSESSMENT OF ANTENNA GAIN AND POINTING, AND CALIBRATION OF RADIO SOURCES

P H Richter and D J Rochblatt

Jet Propulsion Laboratory, USA

1. INTRODUCTION

The NASA JPL Deep Space Network (DSN) of large, dual reflector antennas is subject to continuing demands for improved performance and reliability as a result of communications, control, and radio science requirements for future missions.

As a consequence, a new generation of 34m Beam Waveguide (BWG) antennas is being added to the existing complement of 34m and 70m cassegrain-like antennas, and X-band (8.42 GHz) and Ka-band (32 GHz) transmitting and receiving systems, the latter utilizing stable, total power radiometers (TPRs), are being implemented throughout the system to complement the existing S-X-band capability.

These developments have in turn established the need for a set of easy to use and reliable tools for the assessment, calibration, and improvement of the performance of a large number of antenna systems.

In this paper we describe a new approach being taken for the measurement of antenna gain and pointing, as well as the calibration of radio sources used in the antenna gain assessment. The companion paper (Part 2) discusses panel and subreflector alignment, and antenna stability.

As a result of a systematic analysis of the entire measurement procedure, with particular attention to the noise characteristics of the TPR plus the tropospherically induced radiometer fluctuations, and the implementation of new techniques for data acquisition and reduction, it has been possible to obtain measurement precision yielding up to an order of magnitude improvement over previous methods in the determination of antenna aperture efficiency, and factors of five or more in the determination of pointing errors and antenna beamwidth. This improvement has been achieved by performing *continuous, rapid raster scans* of both extended and point radio sources.

The significance of improvements in antenna calibration and performance in the DSN can be put in perspective by recognizing that each dB of improvement in the quantity G/T is estimated to be worth about \$80 million in terms of mission support capability [Claus (1)].

In the following section we describe the general requirements for the DSN antenna calibration effort. This is followed by a discussion of current methods, and their shortcomings, and a final section describes the new approach being taken, and some early results.

2. CALIBRATION SYSTEM REQUIREMENTS

The performance of a DSN antenna must be accurately characterized at the time it comes on line as a new instrument. Also, certain characteristics must be checked periodically to maintain performance as well as assess the cause of, and correct for any observed anomaly during normal tracking of a spacecraft.

The initial calibration consists of precision setting of the individual main reflector panels, and subreflector alignment by means of microwave holography, discussed in part 2 of this paper, the determination of aperture efficiency vs antenna elevation angle, and the development of a suitable pointing model to permit accurate antenna pointing.

All of the measurements needed to carry out these calibrations involve far field observations of monochromatic signals transmitted by satellite beacons, or broadband radiation from various celestial sources. Holography measurements are typically carried out at X or Ku-band, based on the availability and elevation of suitable satellite signals, while the remaining measurements utilize S, X, and Ka-band frequencies, depending on the equipment planned for the particular antenna under test.

In all cases some form of sampling of the source radiation as a function of antenna offset from [the source is carried out, the exact nature of which, as well as the subsequent data processing, determine the precision and accuracy achieved in the overall calibration effort.

In the following section we briefly describe, and point out the deficiencies of the conventional approach that has been used in aperture efficiency and pointing measurements. The remainder of the paper is devoted to a discussion of the approach now being pursued to significantly improve these measurements.

3. CONVENTIONAL APPROACH TO APERTURE EFFICIENCY & POINTING MEASUREMENTS

Antenna aperture efficiency, η , may be defined by the equation

$$\eta = \frac{2kTC_r}{AS}, \quad (1)$$

where k =Boltzmann's constant, T =system noise temperature increase due to the source, C_r =source size correction factor, A =antenna physical area, and S =source flux density. Each of the quantities T , C_r ,

“ and S represents a source of error, and the measurement method used to determine each must thus be addressed in any search for improvement.

3.1 Source size correction factor

The source size correction factor is designed to account for the flux density of an extended source not collected by the antenna, and is best understood with reference to the fundamental radiometric equation from which equation 1 is derived,

$$kT_v(\psi; \theta, \phi) = \frac{1}{2} \eta_v(\psi) A \iint_{\text{source}} B_v(\theta', \phi') P_{n,v}(\psi; \theta' - \theta, \phi' - \phi) d\Omega', \quad (2)$$

where B_v is the source brightness function, $P_{n,v}$ is the normalized antenna power pattern, and (θ, ϕ) are rectangular, angular coordinates relative to the source center [Krauss (2)]. Here, we have been specific regarding the dependence of various quantities on the antenna elevation angle, ψ , and the operating frequency, ν , as well as the fact that the measured system noise temperature increase due to the source, $T_{s,v}$, depends on the antenna pointing.

The integral appearing in equation 2 is the source flux density collected by the antenna, and is smaller than the total source flux density

$$S_v = \iint_{\text{source}} B_v(\theta, \phi) d\Omega, \quad (3)$$

unless the source is much smaller in extent than the antenna main beam, and the antenna is accurately pointed at the source. Equation 2 may be cast into the form of equation 1 by defining the source size correction factor,

$$C_{r,v}(\psi) = \frac{S_v}{S_{\text{coll},v}(\psi)} \geq 1, \quad (4)$$

where

$$S_{\text{coll},v}(\psi) = \iint_{\text{source}} B_v(\theta', \phi') P_{n,v}(\psi; \theta' - \theta, \phi' - \phi) d\Omega' \Big|_{\text{max}} \quad (5)$$

is the *maximum* flux density collected by the antenna, i.e., the antenna temperature field, $T_v(\psi; \theta, \phi)$, must be explored at a given elevation until the maximum value is found. It should be noted that the corresponding coordinates will not be those for the source center unless the source happens to be symmetric.

Equations 4 and 5 imply that the determination of $C_{r,v}(\psi)$ requires a knowledge of the source brightness function and the normalized antenna power pattern. For those circumstances where $C_{r,v}(\psi)$ is within a few percent of 1, the usual approach to its evaluation has been to estimate both of these functions by symmetric gaussians, in which case the oft quoted formula

$$C_r^2 = 1 + (\Theta_s / \Theta_b)^2,$$

where Θ_s and Θ_b are the source and beam widths, respectively, is obtained.

However, many commonly used sources have corrections approaching 100 % for a large antenna operated at high frequency. The 70m antenna value for Virgo A at K_a-band, for example, is calculated to be 1.90, and even at S-band this source has a 70m $C_r = 1.205$ [Richter (3)]. Under these circumstances the computation of the source size correction must be carried out with more realistic functional representations of the source structure, and the source of these has been brightness maps measured with interferometer arrays, or large antennas such as the 100m telescope at Bonn.

It is possible, in principle, to carry out a proper deconvolution of such maps to compute equation 5. I'bus, an average brightness map obtained with an antenna having an equivalent normalized power pattern $P_{0,n}(\theta, \phi)$ is given by

$$B_n(\theta, \phi) = \frac{1}{\Omega_0} \iint B(\theta', \phi') P_{0,n}(\theta - \theta', \phi - \phi') d\Omega', \quad (6)$$

where Ω_0 is the equivalent measuring beam solid angle, and we now drop the explicit frequency and elevation angle notation, and for simplicity assume beam symmetry so that the integral has the form of a convolution. Then, taking the Fourier transform of equations 5 and 6 we have

$$\tilde{S}(\mu, \nu) = \tilde{B}(\mu, \nu) \tilde{P}_n(\mu, \nu),$$

$$\tilde{B}_0(\mu, \nu) = \frac{1}{\Omega_0} \tilde{B}(\mu, \nu) \tilde{P}_{0,n}(\mu, \nu),$$

from which we obtain

$$\tilde{S}(\mu, \nu) = \Omega_0 \frac{\tilde{P}_n(\mu, \nu)}{\tilde{P}_{0,n}(\mu, \nu)} \tilde{B}(\mu, \nu), \quad (7)$$

so that performing the inverse Fourier transform yields S_{coll} . This procedure has in fact been used to generate the C_r values currently used in the DSN for calibration purposes, but the approach has a number of limitations which become serious at high frequencies:

1. Maps are usually not available at the frequency of interest so that an interpolation procedure must be used to estimate a map at the required frequency.
2. Large antennas have significant flexure as a function of elevation angle due to gravitational loading resulting in aberrations that affect the beam pattern, so that one really should have C_r values calculated as a function of elevation (see equation 4).
3. Information on the mapping beam solid angle and shape is often approximate or unavailable in the literature.

An alternative approach is thus called for which eliminates the need for source size corrections, and this approach is described in a following section.

3.2 Flux density

Since source flux densities are determined from the same equation used to determine aperture efficiency, equation 1, all of the sources of error attendant the latter must apply to the former as well. Thus, while the very brightest sources can be measured with a low gain system such as a horn, whose calibration is relatively straightforward, the transfer of information from strong to weak sources which are compact enough to serve as reasonable calibrators for large antennas must be carried out with larger antennas. Then, equation 1 leads to the result

$$\frac{S_1}{S_2} = \frac{T_1 C_{r_1}}{T_2 C_{r_2}}, \quad 8)$$

where the subscripts refer to measurements of two different sources with the same antenna, and we see that not only antenna temperatures, but also source size corrections enter into the calculation of flux density ratios for different sources.

A survey of the literature on *flux density measurements* shows that the use of inaccurate C_r values contributes significantly to the error budget for such measurements [Richter (4)], so that eliminating the need for such a correction would result in a significant increase in the accuracy of flux density determinations.

3.3 Source temperature

The basic method for measuring the system noise temperature increase due to a source involves some form of on-source, off-source subtraction. In the DSN this is presently accomplished by a boresight technique in which the antenna is successively offset in a given direction, say θ , relative to the source, by $\pm 5, \pm 1/2$, and zero half-power beamwidths (H PBW's). The resulting 5 data points are then fitted to a gaussian function plus a linear background to account for the decrease in system noise temperature with elevation, and from this fit, the maximum, or peak source temperature, and θ pointing error and beamwidth are determined. The pointing error is then used to execute an orthogonal boresight in the ϕ direction, and the process repeated as the source is tracked.

While this works well at S-band, it is less satisfactory at X-band, and unsatisfactory at K_a -band, especially with regard to the pointing determination, where, for example, it has been unable to provide the requisite precision to meet the radio science requirements for the Cassini mission to Saturn, scheduled for launch in October, 1997. Additionally, the method is inherently slow since each of the 5 measurements in a given direction requires that the antenna servos and mechanical structure settle at the offset specified before a temperature measurement is made. A further problem is that the gaussian fitting function only approximates the actual profile of the temperature measurement, and for an extended source this approximation may not be very good.

In view of these limitations one would like to have a source temperature measurement of inherently greater accuracy. This would not only improve our knowledge of antenna gain and pointing, but would also improve the calibration of weak sources by the comparison method described above.

In the following section we describe a new approach to the calibration of large, ground based antennas that significantly improves the precision achieved by reducing or eliminating the above noted sources of error inherent with present methods.

4. THE RASTER-SCAN METHOD

The key to reducing the error sources discussed in the previous section lies in making system noise temperature measurements over a finite area of sky including the source, rather than along orthogonal cuts through the temperature profile. Thus, integration of equation 2 over the two dimensional angular field (θ, ϕ) gives

$$k \iint_{\substack{\text{source} \\ \text{+beam}}} T(\theta, \phi) d\Omega = \frac{1}{2} \eta A \Omega S, \quad 9)$$

where Q is the antenna beam solid angle, and we have dropped the explicit frequency and elevation angle notation for simplicity.

If we now consider the application of the above equation to two sources, the equivalent of equation 8 becomes

$$\frac{\iint_{\substack{\text{source} \\ \text{+beam}}} T_1(\theta, \phi) d\Omega}{\iint_{\substack{\text{source} \\ \text{+beam}}} T_2(\theta, \phi) d\Omega} = \frac{S_1}{S_2}, \quad 10)$$

a result independent of source size corrections.

If the source considered in equation 9) is small enough relative to the main beam to be considered a point, then its brightness may be represented by

$$B(\theta, \phi) = S_p \delta(\theta) \delta(\phi), \quad 11)$$

where $\delta(x)$ is the Dirac delta function. Then, equations 4 and 5 show that $C_r = 1$ so that equation 1 becomes

$$\eta = \frac{2kT_p}{AS_p} \quad 12)$$

If the flux density, S_p , of this point source is known, then equation 12 immediately yields the aperture efficiency in terms of the peak source temperature. However, it frequently is the case that point sources bright enough for calibration purposes are also variable, so that one may not have a priori knowledge of S_p . In this case, equation 10 may be used to determine S_p by comparison with an extended, calibrated source whose flux density, S_c , is known. Then, combining equations 10 and 12 we have

$$\eta = \frac{2kT_p \iint T_c(\theta, \phi) d\Omega}{AS_c \iint T_p(\theta, \phi) d\Omega}, \quad (13)$$

which now becomes the fundamental equation for determining aperture efficiency.

The data for the computation implied by equation 13 are the temperature fields $T_p(\theta, \phi)$ and $T_c(\theta, \phi)$ for the point and extended calibration source, respectively, and these are obtained by scanning the antenna beam across the source in a raster pattern, similar to a (non-interlaced) TV scan (see below).

It should be noted here that the ratio of the integrals appearing in equation 13 is, by equation 10, just the ratio of the flux densities for the two sources, i.e., a constant. Thus, the measurement strategy should involve the alternate scanning of the two sources over a small but finite elevation change so that the data points corresponding to each integral, as a function of elevation, can be fitted to a linear, or perhaps quadratic function. Then, it should be found that the ratio of these two fitting functions is constant and equal to S_c/S_p . As a practical matter the extended calibration source 3C274 (Virgo A) and the variable point source 3C273 serve admirably for such a strategy as they have nearly the same R.A.

Substitution of equation 11 into equation 2 gives the result

$$T_p(\theta, \phi) = \frac{\eta AS_p}{2k} P_n(\theta, \phi) = T_p P_n(\theta, \phi), \quad (14)$$

so that the raster scan data set for the point source has a functional dependence determined by the beam pattern plus a background term due to the sky, which may be linearly approximated over the small field scanned. Thus, if we assume that the antenna is in good alignment, there are small system aberrations, and the main reflector is nearly uniformly illuminated, which is close to the truth for the shaped reflector designs of the DSN, then $P_n(\theta, \phi)$ can be well approximated by an asymmetric Airy pattern

$$A(\kappa_\theta \theta, \kappa_\phi \phi) = \frac{2J_1 \sqrt{\kappa_\theta^2 \theta^2 + \kappa_\phi^2 \phi^2}}{\sqrt{\kappa_\theta^2 \theta^2 + \kappa_\phi^2 \phi^2}}, \quad (15)$$

so that the system temperature data set for the point source raster scan has the form

$$T_p(\theta, \phi) = T_{op} A[\kappa_\theta(\theta - \theta_0), \kappa_\phi(\phi - \phi_0)] + T_{op} + a_\theta \theta + a_\phi \phi, \quad (16)$$

where κ_θ and κ_ϕ are beamwidth parameters, θ_0 and ϕ_0 are the pointing errors, and a_θ and a_ϕ are the sky background coefficients for the θ and ϕ directions, and T_{op} is the system operating temperature.

The 8 parameters appearing in equation 16 may be found from a nonlinear, least squares fit to the point source raster scan data, thus giving complete

information on the peak temperature, and pointing errors and beamwidths for the two orthogonal directions corresponding to the scan axes. The precision of the resulting fit will depend on the noise fluctuations present in the temperature data, the scan parameters, and the data processing used, and these are dealt with in the following sections.

4.1 Fluctuations in system noise temperature

Three main sources of fluctuation of system noise temperature can be identified:

1. Thermal noise generated in the radiometer and atmosphere,
2. Gain-bandwidth variations in the radiometer caused by ambient temperature fluctuations of electronic components, especially in the first stages,
3. Fluctuations caused by variations in tropospheric density, especially of water vapor content. This is most significant at Ka-band.

The two-sided power spectral density (PSD) of the output fluctuations of a typical DSN Ka-band radiometer has been measured as a function of fluctuation frequency over the range 6.5×10^{-5} to 0.5 Hz, and the results compared with a model based on the above mechanisms. The results are shown in Figure 1, where curve a corresponds to the radiometer looking at an ambient load and curve b was obtained with it looking at the zenith sky.

Curve c is a fit to curve a decreased by the square of the ratio of the system operating noise temperatures, $T_{op}|_{\text{ambient}}/T_{op}|_{\text{sky}} \cong 14.6$, and curve d corresponds to a statistical model for tropospheric fluctuations for average conditions at the DSN complex at Goldstone, California [Treuhaft and Lanyi (5)].

Curve a, which is constant at high frequencies and follows a $1/f^2$ dependence at low frequencies, corresponds to thermal noise and gain-bandwidth variations, and if these were the only terms present with the radiometer looking at the zenith sky, the data of curve b would follow curve c. There is a significant departure from this however, but when curves c and d are added together the result follows curve b closely, from which we conclude that tropospheric fluctuations play an important role in the total radiometer fluctuations at frequencies below about 0.1 Hz.

Since we are interested in frequencies greater than 10^3 Hz when making gain calibrations, i.e., times of interest are considerably shorter than 1000 sec, we may consider only the high frequency behavior of the Treuhaft-Lanyi model, which has a $1/f^{8/3}$ dependence so that curve b may be represented by the equation

$$S_{T_w}(f) = S_0 + \frac{K_1}{f^2} + \frac{K_2}{f^{8/3}}, \quad (17)$$

where the coefficients for the K_a -band radiometer tested have the values

$$S_0 = 1.50 \times 10^{-4} \text{ K}^2 / \text{Hz}$$

$$K_1 = 1.64 \times 10^{-6} \text{ K}^2 / \text{sec}$$

$$K_2 = 2.36 \times 10^{-7} \text{ K}^2 / \text{sec}^{3/2}$$

corresponding to average weather with the radiometer looking at the zenith sky, and a T_{op} of approximately 100K.

With the above form for the PSD of the fluctuations, one may determine the corresponding standard deviation of the fluctuations. This depends on both the integration time, τ , i.e., the period over which the measurements are averaged by the power meter, and, in view of the nonstationary behavior indicated by equation 17, the total duration of the measurement, T .

It can be shown that the variance of a random process $X(t)$, of duration T , having a high frequency cutoff, is given by

$$\sigma_x^2(T) = 2 \int_0^\infty [1 - \text{sinc}^2(\pi f T)] S_x(f) df, \quad (18)$$

where $\text{sine}(x) = \sin(x)/x$, and $S_x(f)$ is the PSD of the process. If the signal $X(t)$ is continuously averaged over a time interval τ , the resulting PSD is

$$S_{\bar{x}}(f) = \text{sinc}^2(\pi f \tau) S_x(f), \quad (19)$$

so that the variance of the averaged process $\bar{T}_{\text{op}}(t)$, of duration T , is

$$\begin{aligned} \sigma_{\bar{T}_{\text{op}}}^2(\tau, T) \\ = 2 \int_0^\infty [1 - \text{sinc}^2(\pi f T)] \text{sinc}^2(\pi f \tau) S_{\bar{T}_{\text{op}}}(f) df. \end{aligned} \quad (20)$$

The evaluation of this integral for the spectrum given by equation 17 is accomplished by contour integration, with the result

$$\sigma_{\bar{T}_{\text{op}}}^2(\tau, T) \approx \sqrt{\frac{S_0}{7} + \frac{2\pi^2 K_1}{3} + 18.3 K_2 T^{3/2}}, \quad (21)$$

where it has been assumed that the measurement duration is considerably longer than the integration time, i.e., $T \gg \tau$.

The duration of the measurement of interest in the raster scan method depends on the rate at which the data are taken, and the details of the analysis. For example, if one were to operate at a lower frequency than K_a -band, the $T^{3/2}$ term in the above equation, corresponding to tropospheric fluctuations, would be absent, and if a radiometer gain calibration were carried out at the conclusion of each line of the scan, then the appropriate time would be the time required for the execution of a single scan line. Generally speaking, however, T will be the time required for one complete raster, and an important conclusion to be drawn from equation 18 is the need for *short* measurement times. This, perhaps counterintuitive conclusion, has been born out in actual tests as will be shown below.

4.2 Raster scan design

Equation 21, together with the need to avoid settling problems with the antenna mechanical system, suggest that the raster scan should be performed with a continuous motion at a constant, high angular velocity in a given direction, say θ , while discontinuously stepping in the orthogonal direction, again, mimicking a TV scan. This means that the data are taken "on the fly", so that the averaging process referred to above will contribute to a distortion of the signal that must be taken into account.

A second, and related consideration is selection of the sampling interval, t_s . In view of the Fourier transform relationship between the complex, far field amplitude, $U_n(\theta, \phi)$, and the complex aperture field, $C(X, y)$, the scan signal for a single line is absolutely bandlimited.

Thus, for a coherent detection scheme such as that used in the microwave holography system, which also uses a raster scan format, the signal is of the form $VU_n(\dot{\theta}t, @)$, where V is an arbitrary amplitude factor related to the antenna gain, and θ is the constant scan angular velocity, and one may show that the spectrum of this signal has, by virtue of the clearly defined antenna aperture, a sharp cutoff at $f_0 = \dot{\theta}/2\Theta_b$, where $\Theta_b = \lambda/2a \approx$ antenna main beamwidth. This cutoff, moreover, is independent of the main reflector illumination and system aberrations, and depends only on the maximum dimension of the aperture in the scanned direction, $2a$.

Similarly, for the noncoherent detection used in gain measurements, the signal is of the form

$$VP_n(\dot{\theta}t, \phi) = V|U_n(\dot{\theta}t, \phi)|^2,$$

so that its spectrum is given by the autoconvolution of the coherent spectrum, and consequently has a cutoff frequency twice as high.

From the above we infer that Nyquist sampling for a coherent system requires a minimum of one sample per beamwidth, while for a noncoherent system, a minimum of two samples per beamwidth is required.

Also, since the signal spectrum is bandlimited in both cases, a sharp cutoff digital filter can be used to remove noise above the cutoff, and this can then be followed by a suitable Wiener filter to compensate for the distortion introduced by the integration, with no loss of high frequency information.

In order to study the interaction between scan velocity, $\dot{\theta}$, array size, N , and integration time, z , computations have been made of the errors expected in the fitted parameter T_p for a range of values for each of these parameters for a one-dimensional fit corresponding to a single scan line, and the results are shown in Table 1. In all cases the sampling interval, $t_s = 7/2$.

The computed errors in T_p are based on a general, nonlinear least-squares fitting analysis, using equation 21 to estimate the noise standard deviation, and a gaussian beam pattern

$$T_p(\theta) = T_p \exp\left[-\kappa_\theta^2(\theta - \theta_0)^2/2\right] \quad (22)$$

rather than an Airy pattern, for simplicity [Richter (6)].

Also shown in Table 1 are the RMS fitting errors of aperture efficiency vs elevation curves based on quadratic fits to the data for a complete 6 hour pass of the source. These errors are inversely proportional to \sqrt{N} , where N, is the number of complete rasters executed during the pass, each of which yields an estimate of all of the fitting parameters.

It is clear from these results that the best overall precision is obtained with a high scan velocity and small array size. Indeed, it appears from the analysis that the limiting factor may well turn out to be the behavior of the antenna servo system and the dynamic response of the mechanical structure.

5. TEST RESULTS

Table 2 presents a typical early test result based on a single scan line through the source 3C273 with a 34m BWG antenna at K_a -band. The parameters, and their errors obtained from the diagonal elements of the covariance matrix of the fit, are based on fitting the data to equation 16 with $\phi = 0$. The theoretical errors for the scan line are computed as above from a nonlinear, least-squares analysis using equation 21 to estimate the noise standard deviation.

The last two columns show theoretical errors for the 5 point boresight method, described in section 3.3, using the same nonlinear, least-squares analysis, and measured errors obtained under essentially the same conditions as for the scan line test.

It can be seen from the data in Table 2 that the measured parameter errors obtained from the single scan line are considerably smaller than those obtained with the conventional boresight technique. The predicted errors based on the nonlinear, least-squares analysis are seen to be about a factor of two smaller than those measured for the scan line, and roughly the same factor smaller in the case of the boresight measurements, with the exception of the error for T_p , which agrees well with the measurement.

In the former case this can be traced to the inadequacy of the fitting function used. The predicted noise background for the scan line, $\sigma_x = 0.0242$ K, is in very good agreement with the measured value, $\sigma_{T_p} = 0.0250$ K, but the reduced chi-square for the fit is 3.53 ± 0.35 , indicating that a significant part of the parameter errors is the result of using a fitting function that cannot follow the data to within the limit imposed by the random data errors.

There is, in fact, direct evidence that this is the case, in that the complete two dimensional scans that were made of the source showed a small, but clear indication of sidelobe asymmetry, most likely resulting from a small subreflector misalignment existing at the time of the measurement.

6. CONCLUSIONS

A theoretical analysis of gain and pointing calibration methods, together with a realistic assessment of system noise characteristics, has led to the conclusion that significant improvement in performance can be realized by performing rapid, continuous raster scans of point and extended radio sources, and determining temperature and pointing information from two dimensional, nonlinear, least-squares fits of the data to realistic beam patterns.

The method has the further advantage that source size corrections, which presently represent a significant source of error in both gain measurements and source flux density determinations, are not needed since essentially all of the source flux density is collected during the raster scan.

The use of rapid scanning also results in the collection of vastly more data than with conventional techniques, so that errors in gain, or aperture efficiency vs elevation curves can be greatly reduced.

Preliminary measurements at K_a -band, based on one dimensional fitting to single scan line data, are in good agreement with theoretical calculations using measured power spectral density data to predict the background noise during a scan, and using this background noise as input to a nonlinear, least-squares model to predict fitting parameter errors.

Future work will concentrate on the development of real-time, two dimensional Levenberg-Marquardt nonlinear fitting routines, assessment of antenna mechanical system limitations to the scan process, and overall system engineering concerns for the implementation of the method system wide.

7. ACKNOWLEDGMENTS

This paper presents results of research carried out at the Jet Propulsion Laboratory, California Institute of Technology under contract with the National Aeronautics and Space Administration. The authors would like to express their thanks to Stephen Slobin for gathering and making available much of the K_a -band boresight data used in the analysis, and performing the first experimental raster scans with the DSN developmental BWG antenna at the Goldstone Venus sight. Also, thanks go to Scott Stewart and Manuel Franco for taking the K_a -band radiometer spectral data, Tommy Otoshi for engineering assistance with the radiometer, Shervin Shambayati for producing Figure 1, and W. Van Snyder for assistance with the integration of equation 20.

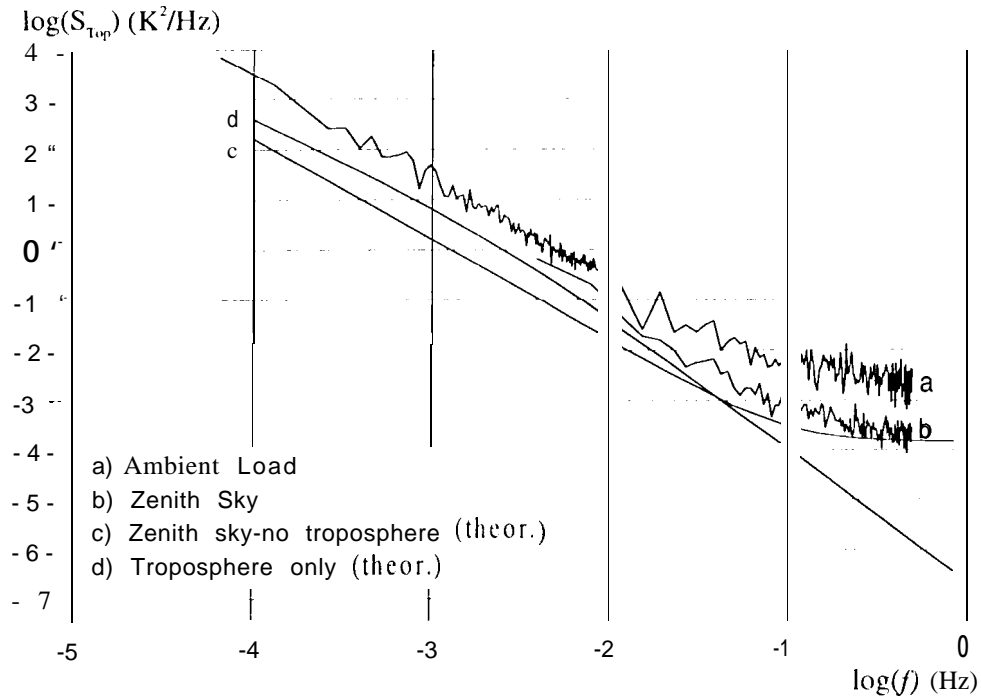


FIGURE 1- Power spectral density of T_{op} fluctuations for K_a -band radiometer

TABLE 1 - Theoretic] errors for the source temperature, T_p , and aperture efficiency vs elevation curve, $\eta(\psi)$, as a function of scan velocity, θ , and array size, N , based on a nonlinear, least-squares fitting analysis for raster scan data acquired with a 34m antenna at K_a -band. The RMS background noise for single scan lines, σ_s , and complete rasters, σ_r , is computed for given scan line durations, t_l , and raster durations, f , from a model based on the measured power spectral density for the radiometer system.

Elevation 90 deg, with troposphere, retrace time = 2sec .

$N=17$	τ , sec	t_l , sec	t_r , sec	$\dot{\theta}$, $\frac{mdeg}{sec}$	σ_l , K	σ_r , K	σ_T , K	$\bar{\sigma}_{FIT}$, %	N_r
	0.1	0.8	47.0	100	0.036	0.068	0.037	0.042	453
	0.2	1.6	61.2	50	0.026	0.074	0.041	0.052	352
	0.4	3.2	88.4	25	0.019	0.094	0.052	0.080	244
	0.8	6.4	142.8	12.5	0.017	0.136	0.075	0.147	151
	1.6	12.8	251.6	6.24	0.022	0.214	0.118	0.309	85
$N=33$	τ , sec	t_l , sec	t_r , sec	$\dot{\theta}$, $\frac{mdeg}{sec}$	σ_l , K	σ_r , K	σ_T , K	$\bar{\sigma}_{FIT}$, %	N_r
	0.1	1.6	118.8	50	0.037	0.123	0.034	0.060	181
	0.2	3.2	171.6	25	0.027	0.159	0.044	0.095	125
	0.4	6.4	277.2	12.5	0.026	0.232	0.064	0.176	77
	0.8	12.8	488.4	6.24	0.024	0.369	0.101	0.370	44
$N=65$	τ , sec	t_l , sec	t_r , sec	$\dot{\theta}$, $\frac{mdeg}{sec}$	σ_l , K	σ_r , K	σ_T , K	$\bar{\sigma}_{FIT}$, %	N_r
	0.1	3.2	338.0	25	0.038	0.278	0.038	0.115	63
	0.2	6.4	546.0	12.5	0.029	0.405	0.055	0.215	39

TABLE 2- Comparison of errors for source temperature T_p , pointing offset, θ_0 , and HPBW, θ_b , for a single scan line through the point source 3C273, with those obtained with the boresight technique. Theoretical errors are computed from the same nonlinear, least-squares model used to predict the errors in Table 1. The frequency was 32 GHz, and the scan parameters were: $N = 21$, $\dot{\theta} = 8.0$ mdeg/sec, $\tau = 0.8$ sec, $t_p = 0.4$ sec, with a total scan width of 64 mdeg.

Parameters from 1 - dim'l fit	Errors from covariance matrix	Theoretical errors for scan line	Theoretical errors for 5 pt. boresight	Typical observed boresight errors
$T_p = 2.9428$ K	0.0332 K	0.0149 K	0.1416 K	0.14 K
$\theta_0 = 5.3463$ mdeg	0.0898 mdeg	0.0427 mdeg	0.4024 mdeg	0.64-1.23 mdeg
$\theta_b = 17.2025$ mdeg	0.2190 mdeg	0.0986 mdeg	0.4185 mdeg	0.58-0.68 mdeg
$T_{vp} = 114.5558$ K	0.0250 K	0.0242 K	-----	-----

REFERENCES

1. Clauss, R., 1996, "Cost to Double the DSN's X-band G/T," JPL IOM RCC 96-055
2. Krauss, J., 1966, "Radio Astronomy," McGraw-Hill, Inc., New York
3. Richter, P., 1994, "DSN Radio Source List for Antenna Calibration," JPL Dec. No. D-3801
4. Richter, P., 1996, "Radio Flux Density Calibrators for the DSN," JPL IOM 3393 -PHR-01- 1996
5. Treuhaft, R. N., and Lanyi, G. E., 1987, "The effect of the dynamic wet troposphere on radio interferometric measurements," Radio Science, 22, no. 2, 251-265
6. Richter, P., 1995, "Estimating Errors in Least-Squares Fitting," TDA Progress Report 42-122, 107-137